Pure Appl. Geophys.

DOI 10.1007/s00024-017-1601-3

Pure and Applied Geophysics

The Mw6.5 17 November 2015 Lefkada (Greece) Earthquake: Structural Interpretation by Means of the Aftershock Analysis

E. Papadimitriou,[1] V. Karakostas,[1] M. Mesimeri,[1] G. Chouliaras,[2] and Ch. Kourouklas[1]

Abstract—The 2015 M_w6.5 Lefkada main shock occurred at the south western part of Lefkada Island (Greece), less than 2 years after the occurrence of a doublet along the western part of the nearby Kefalonia Island, Paliki peninsula (on 25/01/2014, with M_w6.1 and 03/02/2014 with M_w6.0) and 12 years after the 2003 M_w6.2 main shock that struck the northwestern part of Lefkada Island. The four failed dextral strike slip fault segments belong to the Kefalonia transform fault zone (KTFZ), the major active boundary that bounds from the west the area of central Ionian Islands, namely Lefkada and Kefalonia. It is associated with several known historical earthquakes and is considered the most hazardous area in the Greek territory. The KTFZ fault segments are characterized by high slip rates (of the order of tens of millimeters per year), with maximum earthquake magnitudes up to 6.7 for Lefkada and 7.2 for Kefalonia fault zone, respectively. The double difference location technique was employed for relocating the aftershocks revealing a seismogenic layer extending from 3 to 16 km depth and multiple activation on well-defined fault planes, with strikes that differ than the main rupture and dips either to east or to west. This implies that strain energy was not solely released on a main fault only, but on secondary and adjacent fault segments as well. The reliable definition of their geometry forms the basis for the structural interpretation of the local fault network. The aftershock spatial distribution indicates three main clusters of the seismic activity, along with activation of smaller faults to an extent of more than 50 km. A northeasterly striking cluster is observed to the north of the main shock epicenter, with a remarkable aftershock density. The central cluster is less dense than the previous one with an epicentral alignment in full accordance with the strike provided by the main shock centroid moment tensor solution, and is considered as the main rupture with a length of 17 km. The third cluster, encompassing a large number of aftershocks, is located in the offshore area between Lefkada and Kefalonia Islands with a NE–SW epicentral alignment, alike the first cluster. The northeast–southwest striking secondary faults positioned obliquely and in continuation of the main fault segment, reveal that the KTFZ is being deformed in a complex tectonic setting. The presence of faults with this geometry implies strain partitioning and sheds light to new components necessary to be taken into account in the seismic hazard assessment. Stress transfer models of the $M \geq 6.0$ main shocks were investigated and the calculated static stress changes may well explain their sequential occurrence. Static stress changes due to the 2015 coseismic slip were also calculated with the main objective of exploring the aftershock occurrence pattern and it was found as the driving mechanism that triggered the vast majority of the off-fault aftershocks.

Key words: 2015 Lefkada earthquake, aftershock sequence, complex faulting network, stress transfer.

1. Introduction

The area of central Ionian Islands, comprising Lefkada and Kefalonia, is characterized by remarkably high seismic activity, with frequent strong ($M \geq 6.0$) earthquakes that have caused severe casualties and damage during the last six centuries, since historical information is available (Fig. 1). The recurrence of these shocks is remarkably repeated more or less three times per century and for the same fault segment. The twentieth century instrumental destructive earthquakes in Lefkada Island started with the 27 November 1914, $M = 6.3$ main shock accompanied by severe damage distributed onshore near the northwestern coastline. Then it continued with a doublet in 1948, formed by the 22 April 1948, $M = 6.5$ main shock that destroyed the southwestern part of the Island and almost 2 months later, on 30 June 1948, by an $M = 6.4$ event that continued the calamity by hitting the northwestern part of the Island. In historical archives the known repetitive disastrous earthquakes are listed by Stamatelos (1870) who has described thirteen destructions of Lefkada Island between 1612 and 1869 (Papazachos and Papazachou 2003), all taking place in a similar

[1] Geophysics Department, Aristotle University of Thessaloniki, 54124 Thessaloniki, Greece. E-mail: ritsa@geo.auth.gr; vkarak@geo.auth.gr; mmesimer@geo.auth.gr; ckouroukl@geo.auth.gr

[2] Geodynamics Institute, National Observatory of Athens, Athens, Greece. E-mail: g.choul@noa.gr

Published online: 03 July 2017

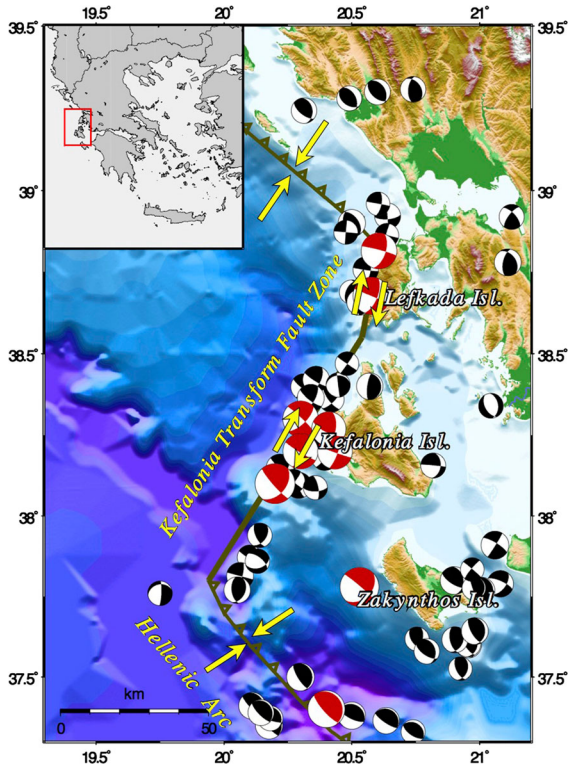

Figure 1
Main geodynamic characteristics of the area of central Ionian Islands shown on a relief map, with the active boundaries shown as *solid lines*. The *arrows* indicate relative plate motion. Fault plane solutions available for the stronger earthquakes are shown as equal area lower hemisphere projections. The beach balls with the compressional quadrants in *red* concern events with $M \geq 6.0$

manner to the instrumental events within the western onshore area.

The spatial distribution of the most disastrous events in Lefkada and Kefalonia Islands, even with an epicentral uncertainty of some kilometers, reveals that they all occurred along a narrow corridor either side of the western coastlines of both Islands, onto fault segments constituting the Kefalonia transform fault zone fault (KTFZ). The latter comprises the boundary between the continental collision to the north (between Adriatic and Aegean microplates) and oceanic subduction to the south (eastern Mediterranean oceanic crust subducted beneath the Aegean). Fault plane solutions of earthquakes that occurred in the last four decades evidenced the dextral strike slip faulting type of the KTFZ (Scordilis et al. 1985; Kiratzi and Langston 1991; Papadimitriou 1993). Under the action of southwest–northeast directed compressional and northwest–southeast extensional stresses, deformation in the study area is dominated by right-lateral strike slip faulting, striking NNE along the Lefkada and NE along the Kefalonia branch of the KTFZ, respectively. The characteristics of these two main branches, and specifically their different strike and dimensions, were afterwards confirmed (Papazachos et al. 1994; Louvari et al. 1999; Kokinou et al. 2006). The change in the strike of the dominant faults is also associated with transtensional and transpressional motion in Lefkada and Kefalonia, respectively.

The last strong earthquake that occurred in Lefkada was in 2003 with M_w6.2 and produced extensive damage along the western coastline along with landslides and rock falls. Its aftershock sequence was thoroughly studied with the use of a dense portable seismological network (Karakostas et al. 2004), which was installed for the first time on the Island and became permanent nowadays. The rupture took place on a right-lateral strike slip fault segment of 16 km length, oriented north-northeast to south-southwest bounding the northwestern coastline of the Island. Based on a reconnaissance study on the 2003 faulting complexity, Karakostas and Papadimitriou (2010) suggested that in addition to the segment that accommodated the main rupture, along strike adjacent fault segments to the south only, and secondary faults near the main rupture were activated as well. Although the majority of aftershock fault plane solutions exhibited mainly strike slip faulting, deviation of this dominant stress pattern was also observed. This deviation is in particular evidenced in the secondary fault segments, which are capable of producing moderate events that in turn may cause appreciable damage. Thus, this type of seismic activity must be viewed with caution in seismic hazard assessment studies. A gap of 10–15 km between the 2003 and 2015 ruptures was found by Ilieva et al. (2016) from analysis of coseismic interferograms without excluding the possible presence of small amount of deformation.

The 2015 M_w6.5 earthquake occurred in the geographical vicinity of the 2003 event, again accommodating right-lateral strike slip motion. It has got the largest reported magnitude for earthquakes in Lefkada Island, and especially in the instrumental era

equal to the magnitude assigned to the first main shock of the 1948 doublet, which also ruptured the southwestern part of the Island. Surface fault expressions were sought but not found by Ganas et al. (2016) in accordance with the coseismic uniform slip model they obtained from inversion of InSAR data and permanent GPS stations. A rupture area containing the main slip zones with a length of 26 km and a width of 7 km is suggested by Choussianitis et al. (2016). Sokos et al. (2016) found that the maximum of slip was mainly identified at the central south part of Lefkada segment on a $\sim$15–20 km long fault almost free of aftershocks, and predominantly at relatively shallow depths (from 3 to 7 km). A kinematic slip model is given by Melgar et al. (2017) suggesting slip concentration mainly to the south of the hypocenter and a fault plane dipping at 65°.

Our analysis involves the spatial relationship of relocated aftershocks to the main rupture of the 2015 event along with the adjacent activated fault segments. Analysis of this sequence from previous publications lacked clear definition of the specific fault segments to which the main shock and the following very intense activity are attributed. Complex earthquake sequences are common in the study area, where multiple adjacent and conjugate faults are contemporaneously activated. The abundance of aftershock activity appears to be correlated with structural complexity, in the sense that aftershock populations reflect fault populations surrounding the major faults. Constraints on the location and geometry of the main rupture and the activated adjacent fault segments are provided by cross sections along the entirety of the aftershock distribution, which is quite heterogeneous spatially. The slip heterogeneity on the fault surfaces is further evidenced by the identification of repeating events. The multiple fault segments failure is explained by stress transfer due to the coseismic slip of the main shock.

2. *Seismotectonic Setting and Historical Seismicity*

It is noteworthy that historical information on earthquakes in the area of central Ionian Islands, although it exhibits the highest seismic activity starts in the fifteenth century, and not beforehand alike in the rest Greek territory, where it starts in the sixth century BC. In particular the first reported event occurred in 1444, when felt reports started to become available. The quantity and quality of these reports depend upon the development of the local cities and the severity of the damage. Reports describing earthquake destructions of Lefkada city are more numerous than for cities in Kefalonia, probably because of the proximity of the causative earthquake to the city. Even though earthquakes along the Kefalonia fault segments are larger in general, some of them are associated with offshore fault segments. This latter could be the reason that the number of earthquakes in early historical archives is smaller for Kefalonia than for Lefkada. Some of the earthquakes were probably not large enough and within adequately close distances from important cities for being reported.

The epicenters are for this latter reason closer to the locations of the important cities where the strongest effects were reported and for which well-

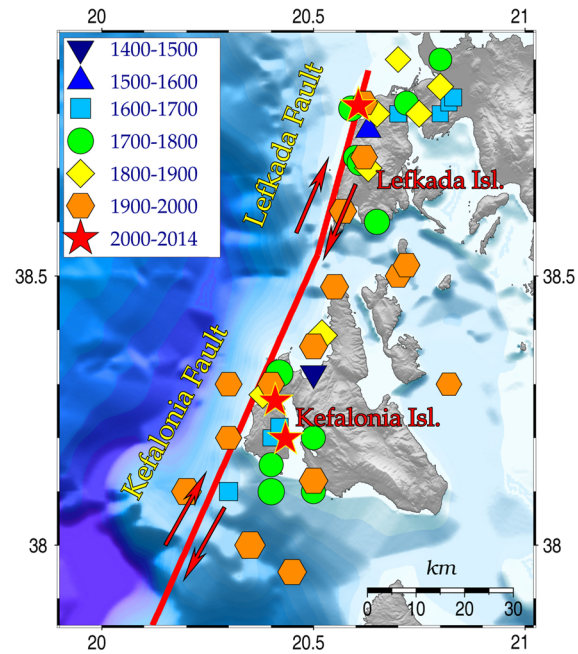

Figure 2
Locations of historical earthquakes with $M \geq 6.0$ that occurred in Lefkada and Kefalonia Islands since the fifteenth century. The inferred traces of the Lefkada and Kefalonia segments of the Kefalonia transform fault zone (KTFZ) are shown with *continuous lines*. Antiparallel *arrows* represent the dextral strike slip motion. Different *symbols* and *colors* have been used to discriminate the seismicity on different centuries

characterized intensity distributions were obtained (Fig. 2). Since the number of cities is quite limited, historical events are concentrated close to the city of Lefkada for Lefkada Island, and the cities of Lixouri and Argostoli for Kefalonia Island. Although it might cause bias, epicentral distribution is rather well correlated with the inferred trace of the KTFZ and in quite good agreement with the positions of instrumentally located events. Magnitudes and locations are estimated from macroseismic observations (Papazachos and Papazachou 2003). Epicenters are generally given to the nearest 0.5° and magnitudes were later revised and are expressed as equivalent moment magnitudes (Papazachos et al. 1997).

Figure 3 shows the sequence of the earthquakes that repeatedly caused damage and have estimated magnitudes $M \geq 6.0$. From an initial observation it can be noticed that Lefkada earthquakes (shown in red) are more abundant before the middle of the nineteenth century, while this changes dramatically afterwards. This is unlikely to be attributed to the seismicity properties but is due to fewer felt events that were reported for Kefalonia (shown in blue) before that time. Only five instrumental (since the beginning of the twentieth century) events with $6.2 \leq M \leq 6.5$ occurred in Lefkada, compared to 14 events with $6.0 \leq M \leq 7.2$ occurring in Kefalonia. From the tight clustering of Kefalonia events, which is perceptibly more intense than the Lefkada ones, a question arises about significant triggering on adjacent fault segments, which seem to have progressively failed, as this could be seen from the spatial distribution in Fig. 2. The clustering preponderance in the occurrence mode of these strong events, has been adequately explained with the stress transfer and triggering (Papadimitriou 2002).

The strong historical earthquakes that are ascribed to Lefkada, have struck either the northern or southern part of the western coastline of the Island, and in some cases they form multiple events. The damage extent suggests that all are related with dextral strike slip faulting onto the Lefkada branch of the KTFZ. The instrumentally recorded shocks exhibit mostly right-lateral motion which changes just north of Lefkada to thrust faulting (Hatzfeld et al. 1995; Louvari et al. 1999). Microseismicity also evidences pure and oblique thrust but in much less extend than the strike slip motion.

3. *Aftershock Relocation and Fault Plane Solutions Determination*

For constraining the model of faults that were activated during this seismic excitation, the accuracy of focal coordinates of the aftershocks provided by the catalogs based on the recordings of the Permanent Regional Seismological Network (1981) and compiled by the Geophysics Department of the Aristotle University of Thessaloniki (GD–AUTh) was refined.

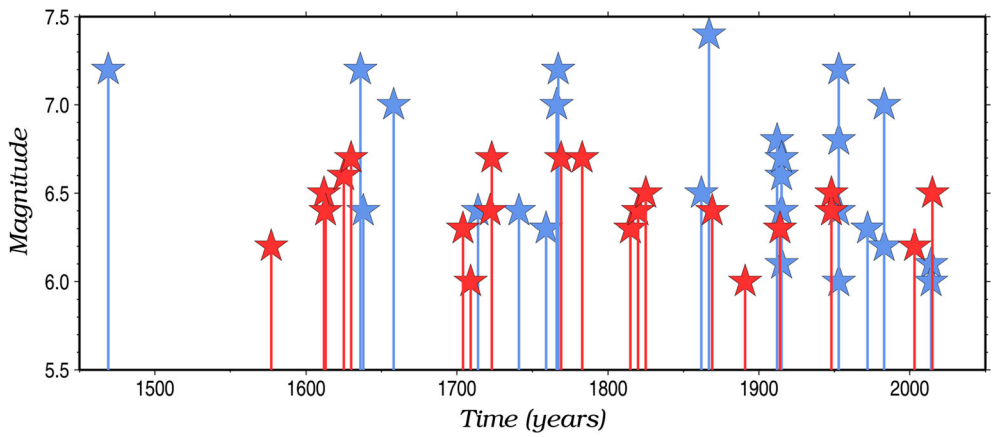

Figure 3
Temporal behavior of strong ($M \geq 6.0$) earthquake activity in central Ionian Islands (*lines* and *stars*, *red* for Lefkada and *blue* for Kefalonia fault branch, respectively)

Table 1

Initial velocity model by Haslinger et al. (1999) and the final one defined in the current study

Haslinger et al. (1999)		Current study	
Velocity (km/s)	Depth (km)	Velocity (km/s)	Depth (km)
5.47	0.0	5.850	0.0
5.50	2.0	5.870	1.0
6.00	5.0	5.980	2.0
6.20	10.0	6.235	6.0
6.48	15.0	6.490	8.0
6.70	20.0	6.525	9.0
6.75	30.0	6.560	11.0
8.00	40.0	6.580	13.0
		6.625	21.0
		6.700	28.0
		8.000	40.0

Aftershocks were relocated using initially an 1-D model along with a recalculated v_p/v_s ratio, which was found equal to 1.86 after applying the Wadati method to a data set in which each earthquake had more than 10 S phases. The 1-D velocity model suggested by Haslinger et al. (1999) is very commonly used for earthquake location in the study area (e.g. Karakostas et al. 2004, 2015), and was used as the starting model for defining a new more appropriate one (Table 1). The VELEST software (Kissling et al. 1994) was employed for this purpose, along with the known $v_p/v_s = 1.86$ ratio and 632 earthquakes located quite close to the main shock, with at least 4 P-phases. The initial model consisted of 41 layers with 1 km thickness each, a decision based on the inefficacy of the VELEST program to automatically adjust the thicknesses of the layers. The procedure was repeated several times until the changes both in the proposed crustal model and station delays are negligible. The final crustal model, defined after merging the layers with equal velocity or taking the average of them when velocity difference was $\Delta v < 0.01$ km/s, consists of ten layers and a half-space below 40 km (Table 1). Station delays were calculated for further refining the location, considering the seismicity in three separate clusters, following a procedure described in Karakostas et al. (2014) and the HYPOINVERSE (Klein 2000) computer program.

Cross correlation followed, which was performed in time domain for close in distance events only, because the waveform similarity decreases with distance (Schaff et al. 2004; Schaff and Waldhauser 2005). An interevent distance threshold less than or equal to 5 km was selected for the locations obtained using the 1D velocity model, to define each individual cluster. Waveforms with 60 s duration and sampling rate of 100 samples per second were taken, and band-passed filtered (2–10 Hz). Then each seismogram was updated with P- and S-wave readings when available. Cross-correlation differential times were calculated for an 1 s window length around P- and S-arrival times and a search over lag ±0.5 s. The final dataset of cross-correlated earthquakes consists of differential times with correlation coefficient (CC) larger than 0.7 and 4 P or 8 S phases for each event pair.

Arrival times of P- and S-waves were used for relocation, along with relative arrival times from waveform correlation (Waldhauser and Ellsworth 2000; Waldhauser 2001) for the three different clusters. Four sets of iterations were performed with five iterations in every set for the inversion with hypoDD software. For the first ten iterations the cross-correlation differential times were down-weighted with a factor of 100 to obtain the locations from catalog data. For the last ten iterations the differential times from catalog data were down-weighted with a factor of 100, for allowing cross-correlation measurements to define small structures. The locations were obtained for each cluster separately and the final catalog contains 1784 events.

A bootstrap method was applied to the final residuals for testing the locations robustness (e.g. Efron 1982; Waldhauser and Ellsworth 2000; Domínguez Cerdeña et al. 2014). For every cluster 200 samples were created by replacement from the final residuals derived from the double difference processing and added to the differential times. The relocation is repeated for each dataset and the results were used to compute the 95% confidence error

Table 2

Median errors of the major/minor axis (X–Y) and the vertical (Z) projection computed by the 95% confidence error ellipse

Direction	North	Middle	South
X	975	490	738
Y	445	250	230
Z	504	398	531

Errors are in meters

ellipse per event (Table 2). The cluster that is located just beyond the northern tip of the main fault and is the most dense one, exhibits the lowest location errors (<500 m), unlike the more northern one, encompassing few events only, the largest ones (~900 m).

The GCMT solution for the main shock shows dextral strike slip faulting along a plane striking at 16° and dipping with 64° to the ESE, with a rake of 179°. Centroid moment tensors for 36 aftershocks with $M \geq 3.5$ were computed in this study with the ISOLA software (Sokos and Zahradnik 2008, 2013) that uses the iterative deconvolution method (Kikuchi and Kanamori 1991) modified for regional distances. The stations selected for the inversion were located at epicentral distances up to 150 km and for this reason the velocity model of Haslinger et al. (1999) was used, as being proper for a regional scale. The inversion was performed for a deviatoric moment tensor and the waveforms are filtered in the frequency range of 0.04–0.08 Hz. Focal mechanisms are all exhibiting right-lateral motion along planes striking NNE–SSW in full agreement with the regional stress pattern (Table 3).

The computation quality was checked by the Focal–Mechanism Variability Index (FMVAR) and the Space–Time Variability Index (STVAR), as suggested by Sokos and Zahradnik (2013). FMVAR is based on the correlation between the observed and synthetic waveforms as a function of trial centroid position. A correlation threshold is set to 0.9 times the maximum correlation and the solutions above that threshold are compared with the optimal solution using the Kagan angle (Kagan 1991). The STVAR measures the size of the space–time area corresponding to the given correlation threshold and is complementary to FMVAR. The solutions with low values of FMVAR (<30) and STVAR (<0.30) are more stable. In our case, the mean values of FMVAR and STVAR are equal to 14 and 0.25, respectively, indicating stability of the moment tensor solution. A minimum number of five stations were used for each solution with a median of nine stations and the mean double couple (DC) of the obtained solutions is 84%. The variance reduction (VR), which reflects the similarity between the synthetic and observed waveforms, is calculated for each event with an overall mean value equal to 0.66 (66%), and the mean condition number (CN), which measures the stability of the inversion, is equal to 3.7 with only two events having a high CN (CN = 10).

4. *Aftershock Distribution and Faulting Geometry*

Figure 4 shows the relocated aftershock spatial distribution where different magnitude ranges are depicted with different symbols and the main shock epicenter by the star. The activity covers a narrow band along and close to the western coastline of Lefkada and Kefalonia Islands, and is developed over an area far beyond either sides of the main shock epicenter. To the south from and near the main shock epicenter, the aftershock distribution appears more sporadic than in other areas where clusters are formed, probably expressing the fact that less aftershocks are located onto the main fault which comprises stress free areas due to a large amount of stress released in the main rupture. To the contrary, stress changes due to the coseismic slip of a main shock trigger off-fault aftershocks, even at large distances from the main rupture plane (Karakostas et al. 2003, 2004, 2014, 2015; for examples from Greek territory). We consider this stress free area as the main rupture with a length of 17 km, smaller than what scaling relations between fault length and magnitude predict.

Beyond both tips of the main rupture aftershocks form clusters that are striking at a slightly different direction. This implies discontinuities in the formation of the secondary faults with different geometry that have been activated during this seismic excitation. For instance, to the north of the main shock epicenter a rather NE-striking cluster with the highest aftershock density appeared soon after the main shock occurrence and persistently continues for several months encompassing the majority of the M4.0 aftershocks. Far beyond its northern tip a smaller cluster is distinguished, along with sparser activity offshore the northwest Lefkada coastline. The second major aftershock concentration is observed in the offshore area between Lefkada and Kefalonia Islands, to the adjacency of the southern tip of the main rupture, with again a rather NE strike. It comprises

Table 3

Information on the fault plane solutions determined in the current study along with the one of main shock as it has been taken from the gcmt determination

S/N	Origin time		Epicenter		Depth (km)	M_o (N × m)	M_w	Fault plane 1			Fault plane 2			*P*-axis		*T*-axis	
	Date	Time	Lon (°E)	Lat (°N)				Strike (°)	Dip (°)	Rake (°)	Strike (°)	Dip (°)	Rake (°)	Azimuth	Dip	Azimuth	Dip
1	20151117*	07:10:07.31	38.6643	20.5845	13.9	$7.150\ 10^{18}$	6.5	22	64	179	113	89	26				
2	20151117	11:57:25.14	38.6960	20.6095	2.0	$9.587\ 10^{15}$	4.6	128	85	−40	221	49	−174	77	30	182	24
3	20151117	12:37:54.56	38.6937	20.6088	3.0	$1.829\ 10^{16}$	4.8	299	88	22	209	67	178	72	15	167	17
4	20151117	19:39:34.88	38.6999	20.6105	5.0	$2.288\ 10^{15}$	4.2	318	78	30	221	59	166	87	12	184	30
5	20151117	20:52:26.98	38.8883	20.5827	5.0	$1.755\ 10^{15}$	4.1	194	78	−168	101	78	−12	58	17	148	0
6	20151117	05:18:14.38	38.5009	20.5277	5.0	$7.074\ 10^{15}$	4.5	345	63	158	85	70	28	214	5	307	34
7	20151118	08:58:37.05	38.5924	20.5697	8.0	$2.605\ 10^{14}$	3.5	298	88	−27	29	63	−178	250	20	346	17
8	20151118	12:15:38.41	38.8430	20.6010	9.0	$3.533\ 10^{16}$	5.0	195	76	−166	102	77	−13	59	18	149	0
9	20151118	13:03:14.57	38.7227	20.6230	3.0	$2.408\ 10^{16}$	4.9	205	65	−159	106	71	−25	65	31	157	4
10	20151118	18:30:07.12	38.7201	20.6176	2.0	$2.667\ 10^{15}$	4.3	25	87	−171	295	81	−2	251	7	160	4
11	20151119	02:07:30.10	38.7061	20.6042	3.0	$2.128\ 10^{14}$	3.5	109	87	−20	200	70	−177	63	16	156	12
12	20151119	02:47:08.40	38.7140	20.6044	7.0	$7.531\ 10^{14}$	3.9	106	74	39	4	51	160	231	15	333	38
13	20151119	13:52:24.73	38.7068	20.6239	1.0	$4.546\ 10^{14}$	3.7	288	57	−16	27	76	−146	252	34	153	13
14	20151119	17:45:55.06	38.4660	20.4863	6.0	$7.456\ 10^{14}$	3.8	217	87	−161	126	71	−3	84	16	350	11
15	20151120	03:01:54.07	38.7987	20.5988	4.0	$3.131\ 10^{15}$	4.3	95	70	−30	197	62	−157	54	35	147	6
16	20151120	03:05:28.53	38.5001	20.4914	2.0	$6.456\ 10^{14}$	3.8	118	59	−14	235	77	−148	82	31	344	12
17	20151120	03:10:19.33	38.4613	20.4803	6.0	$2.253\ 10^{14}$	3.5	212	87	−174	122	84	−2	78	6	347	3
18	20151120	05:12:24.76	38.4668	20.5021	6.0	$2.323\ 10^{16}$	4.9	300	87	−34	31	55	−177	250	25	351	22
19	20151120	08:14:16.36	38.7149	20.6246	3.0	$2.199\ 10^{14}$	3.5	215	72	−177	125	87	−17	79	14	172	10
20	20151120	09:33:15.05	38.6243	20.5754	6.0	$1.014\ 10^{16}$	4.5	20	75	172	112	82	15	245	5	336	16
21	20151120	10:37:14.95	38.4600	20.4741	5.0	$2.881\ 10^{14}$	3.6	53	83	−171	322	81	−6	278	11	188	2
22	20151120	18:07:37.44	38.4604	20.4746	7.0	$1.270\ 10^{14}$	3.3	47	74	174	139	84	16	272	7	4	16
24	20151121	00:41:56.18	38.7055	20.6288	1.0	$9.316\ 10^{15}$	4.6	211	68	−165	116	76	−21	73	25	165	5
25	20151121	01:58:25.79	38.5999	20.5844	11.0	$2.202\ 10^{15}$	4.2	293	79	−36	31	54	−167	246	33	347	16
26	20151121	07:16:43.50	38.7183	20.6234	2.0	$8.606\ 10^{14}$	3.9	202	79	−176	111	86	−10	67	10	158	5
28	20151123	09:30:01.94	38.5257	20.5347	9.0	$1.835\ 10^{15}$	4.1	59	66	12	324	78	156	14	8	280	25
29	20151124	09:39:05.25	38.7154	20.6195	9.0	$2.499\ 10^{15}$	4.2	100	75	40	358	51	161	225	15	327	38
30	20151124	11:56:21.52	38.3730	20.4670	2.0	$7.790\ 10^{14}$	3.9	192	45	−178	101	89	−44	47	31	156	29
31	20151125	03:14:47.17	38.5220	20.5521	6.0	$2.180\ 10^{15}$	4.2	44	54	−20	146	73	−142	11	38	272	12
32	20151129	00:20:44.18	38.7185	20.6251	2.0	$1.799\ 10^{15}$	4.1	203	70	176	294	86	19	67	11	160	16
33	20151129	18:45:14.78	38.7191	20.6354	3.0	$2.435\ 10^{14}$	3.6	214	75	−162	119	72	−15	77	23	347	2
34	20151202	01:44:21.73	38.7004	20.6108	6.0	$7.326\ 10^{14}$	3.9	323	69	37	218	54	154	88	9	186	41
35	20151204	21:12:29.12	38.6994	20.6179	3.0	$3.936\ 10^{14}$	3.7	311	79	23	216	66	168	82	9	176	24
36	20160104	07:21:45.27	38.3293	20.4145	2.0	$4.501\ 10^{15}$	4.4	14	11	−173	284	89	−78	205	44	3	44
37	20160104	18:00:55.12	38.5926	20.5826	9.0	$3.437\ 10^{15}$	4.3	289	82	−42	26	48	−169	239	35	345	22

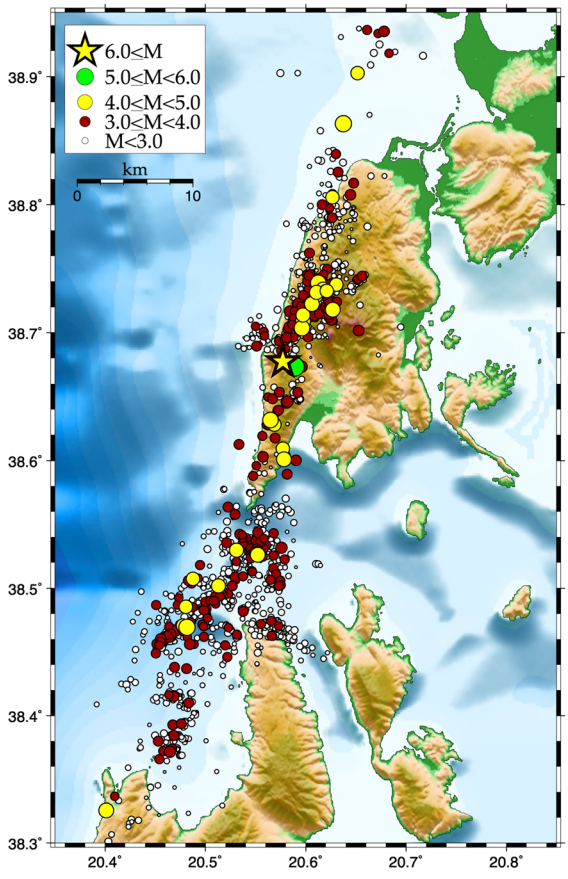

Figure 4
Relocated aftershock locations using the double difference and cross-correlation techniques

several M4.0 aftershocks, and from a visual inspection, a tighter cluster is distinguished, and to a less extent, smaller clusters appear.

For a detailed examination of the aftershock distribution, the aftershock area was visualized with strike parallel and strike normal vertical cross sections, the surface projections of which are shown by the lines in Fig. 5a. The strikes of these active structures were defined by the visual inspection of the map view of the aftershock activity and the related fault plane solutions presented below in this study. These characteristics of the aftershock activity are again obvious and supported by the strike parallel cross section (Fig. 5b), where it appears to occupy an area of approximately 75 km in length with the aforementioned concentrations being also evident. The majority of the aftershocks are at depths between 3 to 14 km, and the main shock focus that is shown by a star is located at a depth of 5 km, along with the largest aftershock (green circle). Although it is expected that the main rupture initiates at the lower part of the seismogenic layer, as predicted by a shear zone model (Scholz 2002) and met in the vast majority of aftershock sequences in Greece and worldwide, this focal depth is in accordance with the location of the maximum slip patches found by Choussianitis et al. (2016). As it has been noticed in the map view, an area with very sparse hypocenter distribution is distinguished at the middle of the cross section that starts from the main shock hypocenter and is bounded by the two major and denser clusters, with a total length of 17 km. This observation led us to conclude that the main rupture propagated unilaterally from the main shock focus to the south, most of its surface is slip free after the main shock and for this reason it comprises only a few aftershocks, whereas we might speculate that beyond its both tips stress transfer triggered intense off-fault aftershock activity.

The smaller magnitude ($M < 3.0$) earthquakes can be found across the entire length of the section, whereas the $M \geq 3.0$ form two distinct and dense clusters on both sides and the immediate adjacency of the main rupture, as well as other smaller clusters. The northeastern cluster abuts the main shock, is the densest one encompassing most of the $M \geq 4.0$ aftershocks, is about 7 km long and extends between 3 and 12 km in depth. The next smaller and sparser cluster shown in the map view farthest from the main shock along the northwestern coast is an almost rectangular patch of 5 km × 5 km dimensions. The cluster located offshore Lefkada encompasses much less events. Lesser accuracy in the deeper hypocentral position for this offshore cluster cannot be ruled out, due to the larger distance of the closest station. The $M \geq 3.0$ earthquakes encompassed in the southern cluster are located in the depth range 5–14 km and the main aftershock cloud has a length of about 12 km. The smaller more southern clusters seen in the map view appear as vertical narrow stripes here.

A vertical cross section (NN′) is constructed for detailing the geometry of the main fault, perpendicular to the main strike of the aftershock zone (PP′), assuming different lengths for the main rupture and considering the seismicity of a seismic stripe at a distance of 6 km either side of the line NN′ (Fig. 6). For a supposed 12 km fault

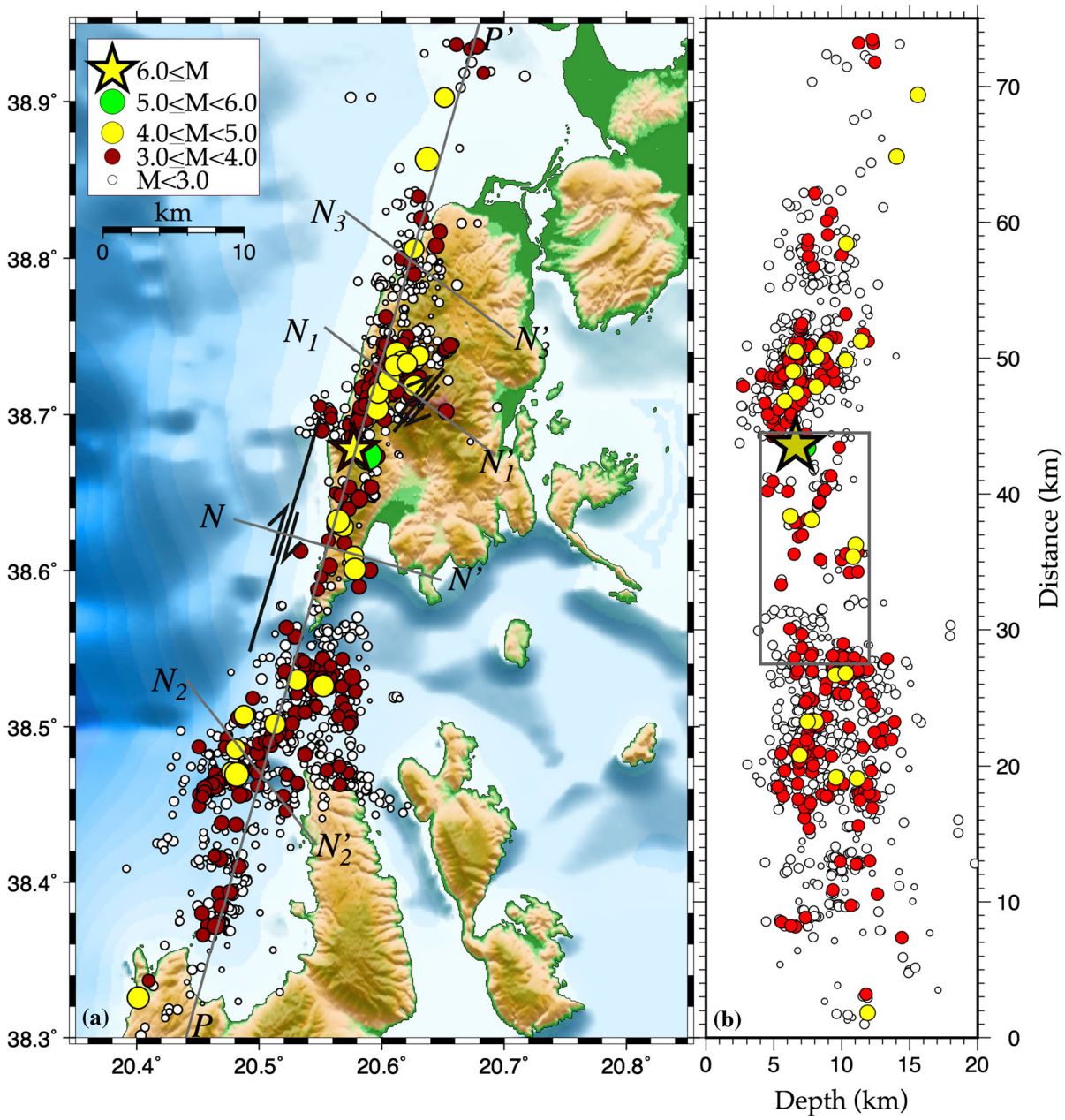

Figure 5

a Map view of the relocated seismicity. The *thick solid line* shows the main rupture extent with the antiparallel *arrows* emphasizing the dextral strike slip motion. The *line* PP′ shows the position of the strike parallel vertical cross section, whereas the NN′, N_1N_1', N_2N_2', and N_3N_3' of the normal ones. The main shock epicenter is depicted by a *star*, **b** Strike parallel cross section along the line PP′. The main rupture area is enclosed by the *rectangle*

length, all aftershocks that are encompassed in the cross section clearly define a plane dipping at a high angle of ~65° to the ESE, at 4–12 km depths, in excellent agreement with the GCMT solution (Fig. 6a). A similar clear picture is obtained when the rupture length is taken equal to either 15 km (Fig. 6b) or 17 km (Fig. 6c). Scattering starts to prevail after the assumed length reaches 20 km (Fig. 6d) where, although the dip to ESE is evidenced, the fault plane can not be clearly defined. This constitutes strong evidence that the rupture length should

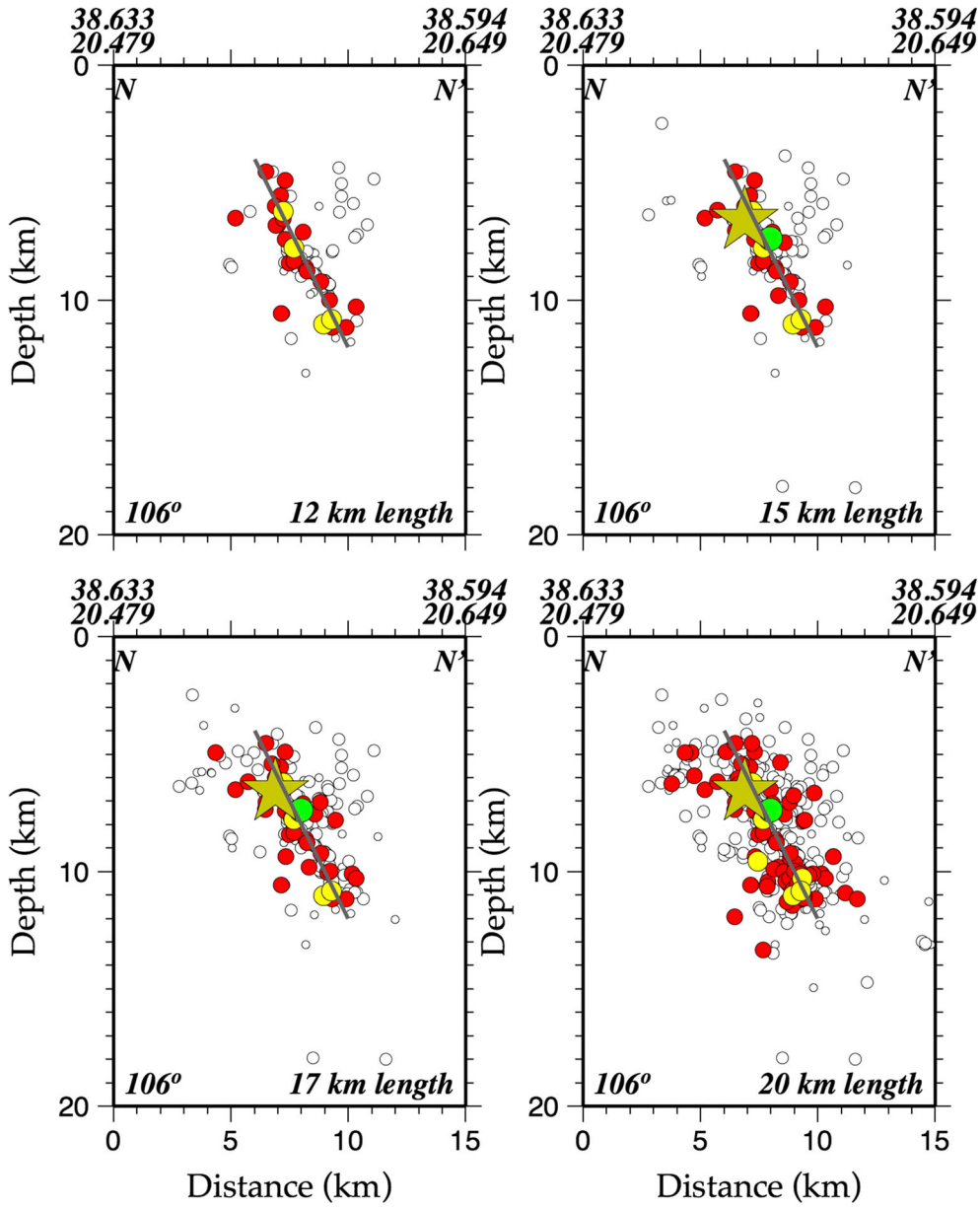

Figure 6
Strike normal cross sections along the line NN′ shown in Fig. 5 for inferred length of the main rupture equal to **a** 12 km, **b** 15 km, **c** 17 km, and **d** 20 km

be less than 20 km, and the length of 17 km that is suggested in this paper is well supported by this observation.

The geometry of the clusters formed by the off-fault aftershock is subsequently analyzed. The cluster next to the northern tip of the main rupture comprises the largest aftershock number in comparison with the other clusters, with about the half of the $M \geq 4.0$ off-fault aftershocks, striking at $\sim 40°$. Its vertical profile (projected onto the line N_1N_1' in Fig. 5), evidences that most $M \geq 3.0$ aftershocks are distributed in focal depths between 3 and 12 km, and lie close to a single plane dipping steeply to the northwest at an angle of more than 70° (Fig. 7). The aggregate orientation of the aftershock zone south of the main rupture is NE–SW alike the strike of the KTFZ at this place. A more detailed inspection, however, discloses that it encompasses smaller clusters

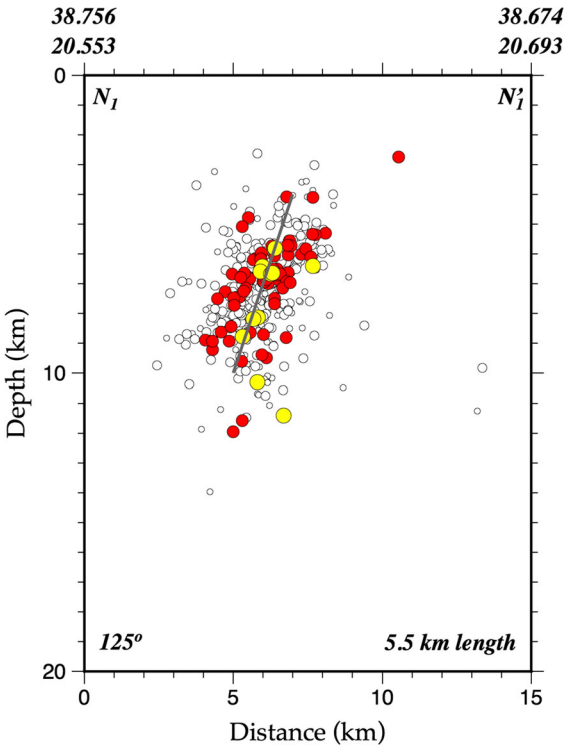

Figure 7
Strike normal cross section along the line N_1N_1' encompassing the earthquakes (5.5 km either side of the section shown in Fig. 5), of the first northern cluster just beyond the northern tip of the main fault

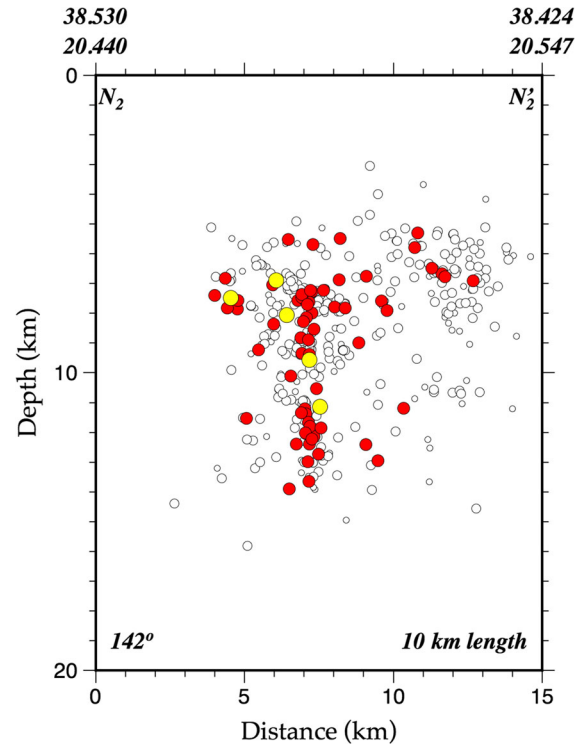

Figure 8
Strike normal cross section along the line N_2N_2' encompassing the earthquakes (10 km either side of the section shown in Fig. 5), of the first southern cluster just beyond the southern tip of the main fault

with different orientation, some of them related to morphotectonic features as the one located at the northernmost part of Kefalonia Island. The vertical cross section in this area, the surface projection of which is the line N_2N_2' in Fig. 5, which is normal to the alignment of epicenters of the $M \geq 3.0$ events and to the mean fault plane solution of this aftershock cluster, reveals a seismogenic layer in depths between 5 and 14 km, with ambiguous dips of the activated fault segments (Fig. 8). A prevalent vertical fault segment is evidenced, and smaller fault patches also appear. These are probably developed in different orientations, and for this reason, their geometrical features are not obviously revealed in the cross sections that were constructed for a certain fault orientation. This is the explanation for the small shallower hypocentral cloud near the southern edge of the section, the geometry of which is not clearly identified. The epicentral alignment of the northern most cluster exhibits almost the same strike with its adjacent cluster, investigated with the cross section along the line N_3N_3' (shown in Fig. 5). It could be speculated that a rather similar dip to the northwest in the cross section along the line to the northwest (Fig. 9). This provides an indication that it does not belong to the 2003 main fault, but it rather constitutes a manifestation of an activated conjugate secondary fault.

The fault plane solutions of the main shock and the 36 aftershocks determined in the present study, information on which is provided in Table 3, are shown in Fig. 10 as equal area lower hemisphere projections. All solutions imply that strike slip faulting is prevailing, although differences in both strike and dip of the nodal planes are noticed. The data set can be easily divided into four distinctive subsets for detailing the faulting pattern, each one comprising closely located events with very similar focal mechanisms, and a mean fault plane solution is determined for each cluster. Close to the main

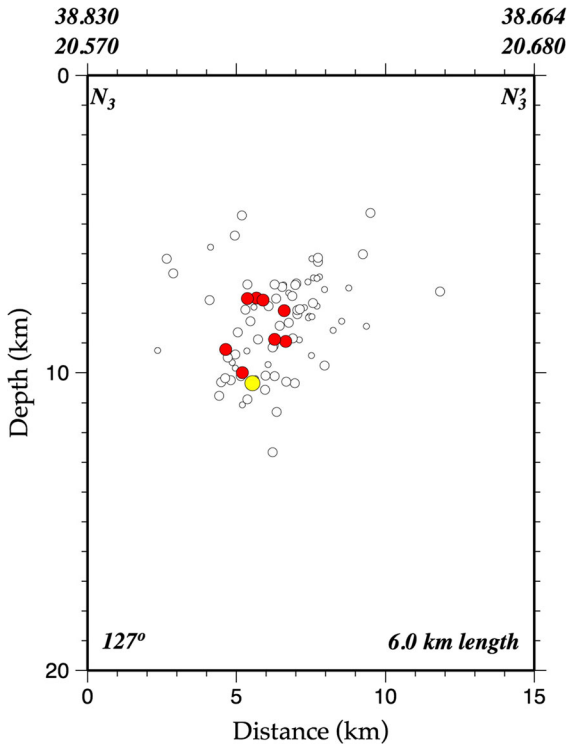

Figure 9
Strike normal cross section along the line N_3N_3' encompassing the earthquakes (6.0 km either side of the section shown in Fig. 5), of second northern cluster just beyond the northern tip of the main fault

shock, four focal mechanisms were determined that are in full agreement with the GCMT solution (cluster numbered 01 in Fig. 10). In the north-eastern cluster (numbered 02 in Fig. 10), the strike differs from that of the main shock, and most importantly, they dip to the northwest. Representative mechanisms were also sought for the two clusters in the southern offshore area, numbered 03 and 04 in Fig. 10, exhibiting very steep nodal planes and are quite different from each other. The cluster 04 exhibits similar features with the mechanisms of the first cluster. The cluster 03 can only be interpreted kinematically and not dynamically, since it is compatible with the orientation of maximum compressional and tensional axes at right angles of the dominant stress pattern. The comparison of the grouped fault plane solutions supports the difference between the different aftershocks clusters.

5. *Identification of Repeating Aftershocks*

During the relocation process, waveform cross correlation was performed for all earthquake pairs over a 7 and 8 s window, respectively. The window values are based on a mean value of S–P time difference multiplied by the velocity ratio (Becker et al. 2006). Thus, the window depends on the epicentral distance of the stations that recorded the earthquake. On the basis of waveform similarity analysis, we detected earthquake clusters with very similar (cross-correlation coefficient $\geq$0.95) waveforms, which are kept and classified as multiplets. An event is considered as a member of a multiplet when it is a doublet with at least one other event in the multiplet (Got et al. 1994). During a 2 month duration of the aftershock sequence, 107 multiplets were identified. Eighty of them (79%) are doublets and twenty-seven comprise 3–11 events. Figure 11 depicts all the events that belong to multiplets of repeating events with at least three members, along with the waveform similarities of three multiplets. Most multiplets are located beyond the southern and northern tips of the main rupture, with the northern concentration being more multitudinous. Only three multiplets are located in a very small area close to the main rupture not undoubtedly associated with it. The occurrence of repeating events with almost the same source could be considered as the consequence of redistribution of stresses in the neighborhood of the main shock and/or afterslip on the main rupture.

6. *Earthquake Triggering in Kefalonia and Lefkada as Inferred from Static Stress Modeling*

The consecutive failure since 2003 of the four adjacent fault segments that are located along the western coasts of Lefkada and Kefalonia Islands and belong to the KTFZ, as it was already mentioned above, with earthquakes of $M_w \geq 6.0$, demands the examination of whether these shocks constitute a cascade triggered by stress transfer. Static stress changes associated with the coseismic slip of each earthquake were determined on the basis of Coulomb failure criterion, according to the equation:

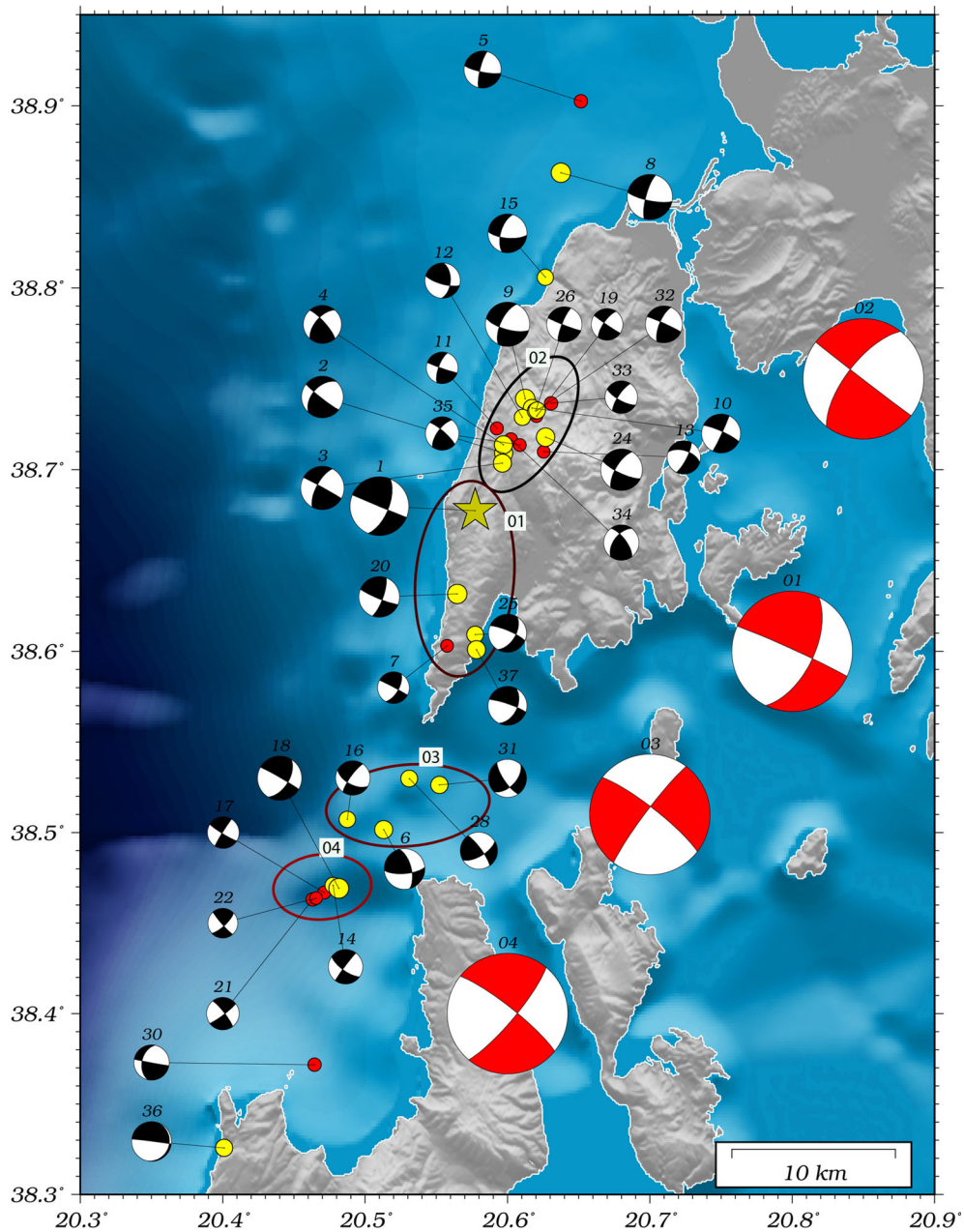

Figure 10
Fault plane solutions determined for the purpose of the present study and shown as lower hemisphere equal area projections. Four distinct clusters are identified and their respective representative fault plane solutions are given to their right, where the compressional quadrants are shown in *red*

$$\Delta\text{CFF} = \Delta\tau + \mu\,(\Delta\sigma + \Delta p) \qquad (1)$$

where $\Delta\tau$ is the shear stress change onto the fault plane (positive in the direction of fault slip), $\Delta\sigma$ is the fault-normal stress change (positive for increasing tensional normal stress), Δp is the pore pressure change in the rupture area, and μ is the friction coefficient, which takes values between 0.6 and 0.8 (Harris 1998 and references therein). A positive value

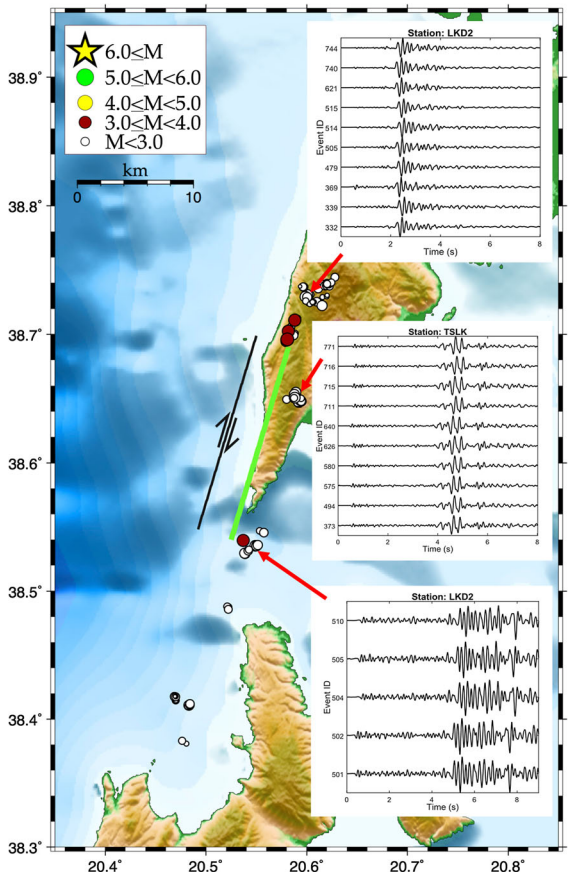

Figure 11
Locations of the three repeating aftershock clusters, along with comparison of the waveforms from a single station for each cluster

of the ΔCFF indicates encouragement for failure and thus triggering of the next rupture, while the negative values indicate rupture inhibition.

The pore fluid pressure is taken unchanged with time, meaning that the Δp depends upon the normal stress change on the considered fault plane (Beeler et al. 2000). The induced changes in the porous medium that result from stress changes under undrained conditions are calculated from (Rice and Cleary 1976):

$$\Delta p = -B\frac{\Delta\sigma_{kk}}{3} \qquad (2)$$

where B is the Skempton's coefficient ($0 \leq B < 1$) and $\Delta\sigma_{kk}$ is the summation of diagonal elements of the induced stress tensor. The value of B is nearly zero when the pores are filled by air, and typically between 0.5 and 1.0 for fluid-saturated rock and close to 1.0 for fluid-saturated soil. Sparse experimental determinations of B for rocks indicate a range from 0.5 to 0.9 for granites, sandstones, and marbles (Rice and Cleary 1976).

Stress changes were calculated according to the faulting type of the next earthquake in the sequence of the four events, whose triggering is inspected. Taking into account that stress is a tensorial quantity, the calculations must be examined in the context of the specific faulting type, i.e., strike, dip, and rake. A particular location could be situated in a stress enhanced area when the stress changes are calculated for an N–S striking dextral strike slip fault for example, while it would be located inside negative stress changes area for a different faulting style. The shear modulus and Poisson's ratio were taken equal to 3.3×10^5 bar and 0.25, respectively, in all calculations of this study.

The rupture models required for the ΔCFF calculations are approximated with rectangles embedded in the Earth's brittle crustal layer. Fault surfaces are defined by their geometrical parameters, their length, L, and width, w, and the parameters provided by the fault plane solutions. The dimensions of the coseismic ruptures are well constrained by aftershock relocation and elaboration of their 3-D distribution (after Karakostas et al. 2004 for the 2003 Lefkada main shock; Karakostas et al. 2015 for the 2014 Kefalonia doublet). The values of scalar moment for each earthquake were adopted from the global centroid moment solutions (http://www.ldeo.columbia.edu/~gcmt/) and an average slip was calculated from these values and fault dimensions (Table 4) considering rigidity equal to 3.3×10^5 bar (the same as above). Values of $\mu = 0.75$ and $B = 0.5$ were considered, which result in an apparent coefficient of friction $\mu' = \mu(1 - B) = 0.375$, very close to $\mu' = 0.4$ suggested by Papadimitriou (2002) who tested the influence of various values for μ' in the study area. Figure 12a evidences that the 2003 main shock created a lobe of positive static stress at the locations of the 2014 and 2015 earthquakes. The first 2014 main shock created large values of positive stress changes at the location of the second 2014 main shock (Fig. 12b), while both 2014 main shocks have not changed substantially the values of positive stress changes at the location of the 2015 main shock,

Table 4

Rupture models for the earthquakes included in the stress calculation model

Date	Time	Latitude (φ° N)	Longitude (λ° E)	L (km)	U (m)	M_w	Mechanism		
							Strike	Dip	Rake
2003, Aug. 14	05:14:55	38.815	20.606	16	0.60	6.2	18	60	−175
2014, Jan. 26	13:55:41	38.199	20.434	13	0.38	6.1	20	65	177
2014, Feb. 03	03:08:44	38.269	20.410	11	0.52	6.0	12	45	154
2015, Nov. 17	07:10:07	38.6775	20.5773	17	1.43	6.5	16	64	179

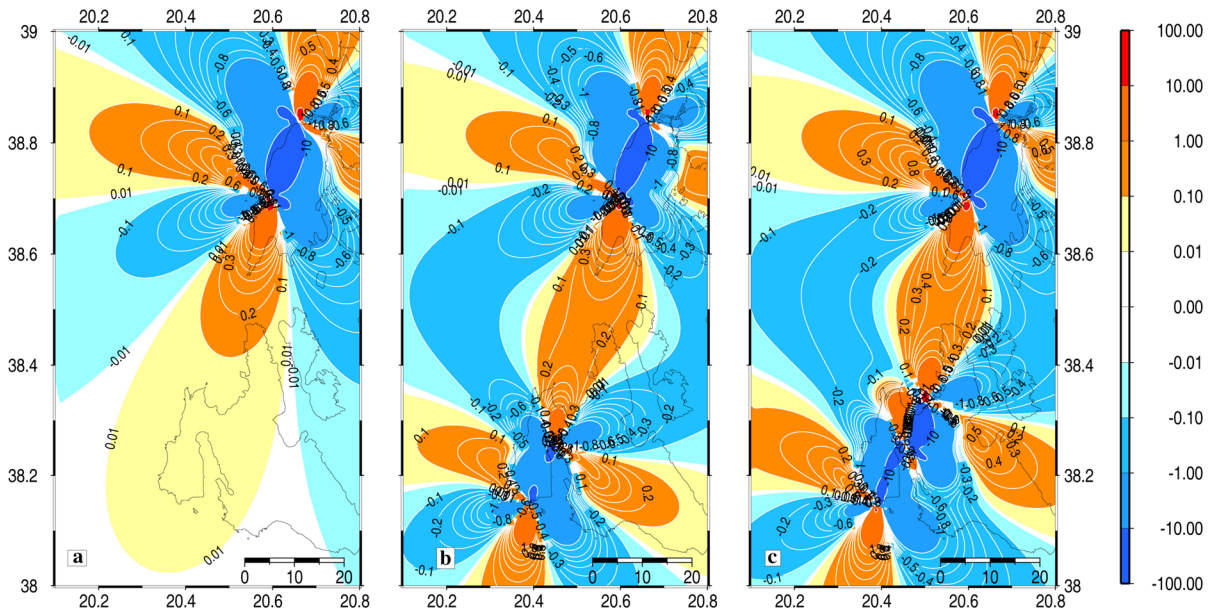

Figure 12

Coulomb stress changes due to the coseismic slips of the $M \geq 6.0$ main shocks that occurred in central Ionian Islands since 2003, calculated at a depth of 8 km. Changes are according to the color scale on the right (in *bars*) and by the numbers in the contour *lines*. The stress field is calculated according to the faulting type of the 2015 main shock and is due to the coseismic slip of **a** the 2003 main shock, **b** the 2003 and the first 2014 main shock, and **c** the 2003 and both 2014 main shocks

as they have been created initially by the 2003 main shock (Fig. 12c).

Coulomb stress changes due to the coseismic slip of the 2015 main shock were calculated to seek for possible triggering of the off-fault aftershock clusters. A dislocation plane with strike = 16°, dip = 64°, and rake = 179° was considered for the causative fault, where only the strike is slightly different than the GCMT solution (22°/64°/179°), because the one chosen here is in better agreement with the strike defined by the aftershock delineation at the location of the main fault. Figure 13a shows the spatial distribution of the Coulomb stress changes resolved for a receiver fault with the same characteristics with the main fault. The on-fault aftershocks are located inside an area of negative stress changes, as it is expected, because a uniform mean slip model was considered.

We then defined two different types of receiver faults, representative of the northeastern and the southern clusters. The stress pattern in Fig. 13b was calculated according to the mean fault plane solution of the northeastern cluster (215°/70°/−170°). A visual inspection reveals the inclusion of the vast majority of the northeastern aftershock inside the lobe where the positive stress changes show values equal to or larger than 1.0 bar. The good match for

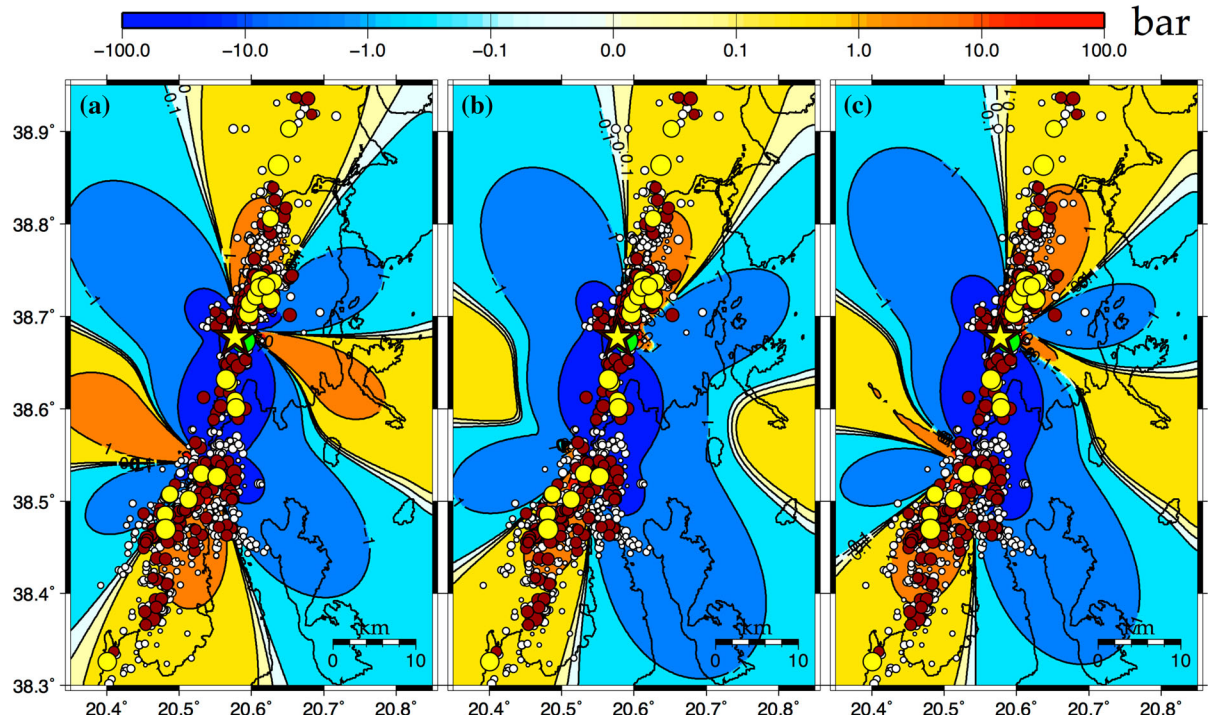

Figure 13
Coulomb stress changes due to the coseismic slip of the 2015 Lefkada main shock calculated at a depth of 8 km. Changes are according to the scale of the top (in *bars*) and by the numbers in the contour *lines*. The main shock epicenter is depicted by a *star* and the ones of aftershocks by *circles*, scaled according to the magnitude. The stress field is calculated according to the faulting type of **a** the main shock, **b** the representative fault plane solution of the northern cluster, and **c** the representative fault plane solution of the southern cluster

the northeastern aftershocks indicates that the stress transfer imparted by the main shock promoted failure in this fault zone with orientation prominently different from the main shock rupture. The stress pattern calculated for the faulting type prevalent for the cluster located between Lefkada and Kefalonia Islands (35°/70°/−170°) is shown in Fig. 13c. As it has been evidenced for the northeastern cluster, the southern cluster took place at an area where the Coulomb stress was calculated to have increased by more than ten bars. It is obvious that off-fault aftershock activity is developed mainly inside the two along strike lobes of positive static stress changes.

For a detailed representation and a quantitative evaluation of the triggering mechanism, the values of the ΔCFF were calculated at each aftershock focus. Figure 14a shows a histogram of these values calculated at the focus of each aftershock belonging to the northern cluster when the faulting type of the receiver fault is considered the same as the one of the main fault, whereas Fig. 14b depicts the respective histogram when the representative fault plane solution of the northern cluster is considered as receiver plane. In the first case, 22.4% of the aftershocks obtained negative stress changes, while this percentage became much smaller and equal to 5.0% when the stress field was calculated according to the faulting type of the representative fault plane solution. The same procedure was repeated for the southern cluster where it was found that 35.5% of the aftershocks were generated at the locations with negative Coulomb stress changes when they were calculated for the faulting plane of the main shock (Fig. 15a), and this percentage diminished to 24.4% when the calculations were performed for the mean fault plane solution of the southern cluster (Fig. 15b). A paired sample *t* test was performed to investigate whether changes in the calculated ΔCFF values are statistically significant when they are resolved for a rupture same as the causative fault and then for the

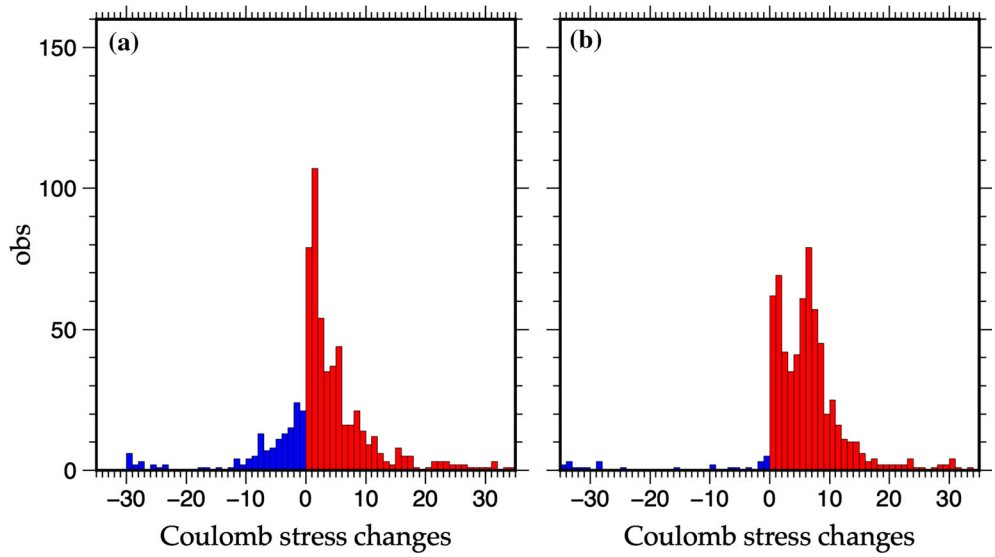

Figure 14
Histogram of the Coulomb stress changes at the foci of the aftershocks of the northern cluster when they are calculated according to **a** fault plane solution of the main shock and **b** representative fault plane solution of the northern cluster

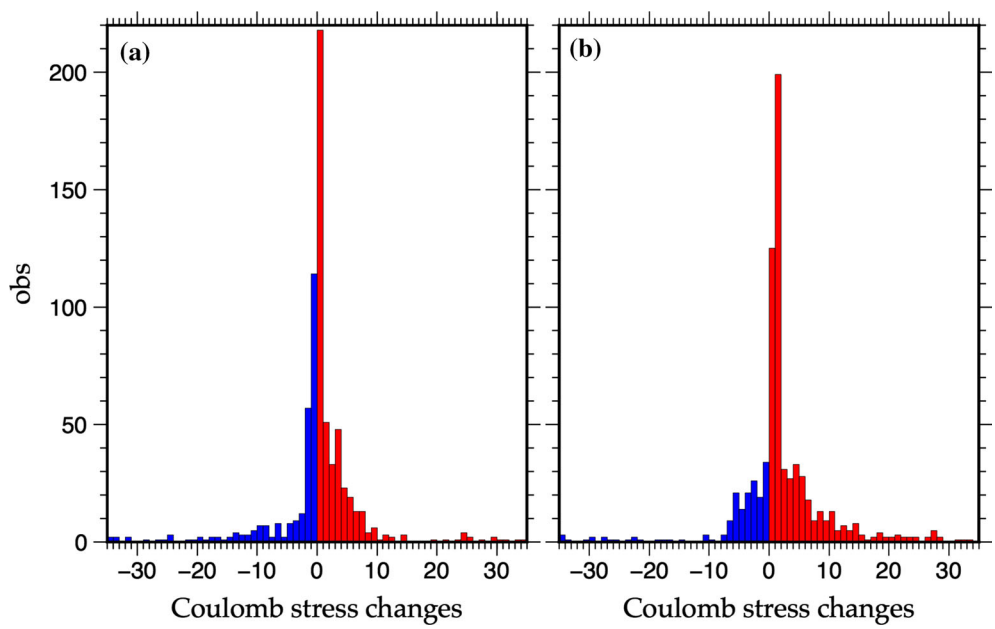

Figure 15
Histogram of the Coulomb stress changes at the foci of the aftershocks of the southern cluster when they are calculated according to **a** fault plane solution of the main shock, and **b** representative fault plane solution of the southern cluster

representative faulting type. In both the cases, it was unveiled the difference which is statistically significant. The fact that this latter percentage is larger than the one of the northern clusters is probably attributed to the fact that the northern cluster is most probably associated with one fault segment, whereas the

southern seismicity may be associated with smaller segments with differences in their style of faulting, as it was already mentioned above. It concerns the transition zone between Lefkada and Kefalonia Islands which may consist of small parallel step-over faults according to Karakostas et al. (2015).

7. Conclusions and Discussion

The source and aftershock activity of the 17 November 2015, $M_w = 6.5$ Lefkada main shock is investigated aiming to shed light on the complex fault network consisting of the main causative fault and the activated neighboring fault segments. The activity took place and produced damage along the southwestern shoreline and is associated with the southern branch of Lefkada Fault Zone. The 2015 rupture reflects the right-lateral strike–slip motion that takes place along the KTFZ, the major fault zone of the central Ionian Islands area where four strong ($M_w \geq 6.0$) earthquakes occurred in ~ 12 years, each being associated with along strike segments of the KTFZ. The sequence of strong ($M \geq 6.0$) events that started with the 2003 Lefkada earthquake associated with a fault segment along the northwestern coastline of Lefkada Island and then the 2014 doublet associated with the failure of two adjacent fault segments along the Paliki peninsula in Kefalonia Island.

High-precision aftershock relocation using a well-constrained velocity model along with waveform cross correlation was performed, providing a detailed spatial profile of the aftershock sequence evolution. These locations allowed refined and more reliable picture in comparison with those presented in the related publications mentioned in the introductory section. The aftershock distribution of the earthquake of 17 November 2015 reveals that the main slip is associated with a fault of about 17 km long, smaller than predicted from scaling laws, along the southwestern coast of Lefkada Island. The orientation of the aftershock distribution at this location coincides with the NNE–SSW strike suggested from the centroid moment tensor solution. The rupture propagated mostly unilaterally, from north to south, and the lack of dense aftershock activity associated with the main fault implies quite uniform coseismic slip distribution. This might be attributed to small distances within asperities, which is one of the main factors controlling whether a major earthquake will occur, which could trigger each other during a single event and might generate a larger earthquake collectively. The location and extent of the main rupture as is defined by aftershocks, fault plate solutions, and repeating events is in good agreement with macroseismic observations, GPS, and InSAR images.

Two distinctive and very energetic clusters were formed beyond both fault tips, with orientations obliquely positioned to the main fault, forming en-echelon fault planes, reflecting the complex fault geometry in this region, and giving rise to further examination with more data elaboration for detailing its geodynamic complexity. The southward expansion of the seismicity with dense aftershock clouds between Lefkada and Kefalonia was also observed after the 2003 rupture and is adequately explained with stress transfer between along strike adjacent fault segments (Karakostas et al. 2004). This could not be attributed to a jump of the 2003 rupture at a distance of ~ 40 km, a consideration that was abrogated by the InSAR model of Ilieva et al. (2016), as well as by the good agreement between geodetic and seismological moments.

The focal mechanisms calculated for 36 aftershocks with $M_w \geq 3.3$ exhibit predominantly strike slip motion, and reflect local details of the stress pattern. Some of these mechanisms are different than the one of the main shock, manifesting motion on faults with different characteristics. In particular, the resolved fault plane solutions assigned to the activated adjacent fault segments evidence that the active deformation in the study area is expressed in more complex mode than a unique dextral strike slip motion onto the major segments composing the KTFZ.

The distribution of aftershocks implies static stress transfer to secondary faults accommodating deformation during the activation of the main faults in a fault population. Positive static stress changes were calculated at the aftershock hypocentral locations of the adjacent to the main rupture northern and southern clusters. The stress changes were resolved according to the representative faulting type of the respective cluster and reveal that intense aftershock

activity can be due to stress transfer. Off-fault aftershocks occurred in areas brought closer to failure by some bars, whereas the strongest of them occurred in short time lags. Gomberg et al. (2003) found that dynamic triggering due to rupture directivity results in asymmetric seismicity distribution with distinctly increasing seismicity in the direction of rupture propagation. In the present case, such preferential increase of the off-fault seismicity was not observed; instead, it was triggered beyond both fault tips, and it was well explained with static Coulomb stress change triggering.

The investigation of the 17 November 2015 earthquake and its aftershock sequence is challenging to shed light on the seismotectonic setting and the complex geodynamics of the area, prerequisite for any reliable seismic hazard assessment study. The complexity of the active structures, as it was already noticed, which in addition to the primary segments of the KTFZ are capable of producing disastrous earthquakes, highlights the need for intensive maintenance and careful analysis of the seismicity. Identification of repeating events highlights the observation that stress redistribution activated the local fault network comprising smaller or larger secondary faults, close to the main rupture. In conclusion, the main shock is associated with a major fault segment of KTFZ, with clearly dextral slip motion, secondary faults are well developed, and active and oblique motion is present, indicating strain partitioning in secondary active structures.

Acknowledgements

The constructive comments of two anonymous reviewers and the editorial assistance of Dr. Sabina Bigi are greatly appreciated. Fault plane solutions data used in this paper came from http://www.ldeo.columbia.edu/~gcmt/ and published sources listed in the references. The stress tensors were calculated using a program written by Deng and Sykes (1997), based on the DIS3D code of S. Dunbar, which later improved (Erickson 1986) and the expressions of G. Converse. The plots were made using the Generic Mapping Tools version 4.5.3 (http://www.soest.hawaii.edu/gmt, Wessel and Smith 1998). Geophysics Department Contribution 896.

References

Becker, D., Meier, T., Rische, M., Bohnhoff, M., & Harjes, H.-P. (2006). Spatio–temporal microseismicity clustering in the Cretan region. *Tectonophysics, 423,* 3–16. doi:10.1016/j.tecto.2006.03.022.

Beeler, N. M., Simpson, R. W., Hickman, S. H., & Lockner, D. A. (2000). Pore fluid pressure, apparent friction and Coulomb failure. *Journal of Geophysical Research, 105,* 25533–25542.

Choussianitis, K., Ozgun Konca, A., Tselentis, G.-A., Papadopoulos, G., & Gianniou, M. (2016). Slip model of the 17 November 2015 $Mw = 6.5$ Lefkada earthquake from the joint inversion of geodetic and seismic data. *Geophysical Research Letters*. doi:10.1002/2016GL069764.

Deng, J., & Sykes, L. (1997). Evolution of the stress field in Southern California and triggering of moderate size earthquakes: a 200-year perspective. *Journal of Geophysical Research, 102,* 9859–9886.

Domínguez Cerdeña, I., del Fresno, C., & Gomis Moreno, A. (2014). Seismicity patterns prior to the 2011 El Hierro eruption. *Bulletin of the Seismological Society of America, 104,* 567–575. doi:10.1785/0120130200.

Efron, B. (1982). *The jackknife, the bootstrap and other resampling plans*. Philadelphia: SIAM. doi:10.1137/1.9781611970319.

Erickson, L. (1986). User's manual for DIS3D: a three-dimensional dislocation program with applications to faulting in the Earth. Master's Thesis, Stanford: Stanford University. p. 167.

Ganas, A., Elias, P., Bozionelos, G., Papathanassiou, G., Avallone, A., Papastergios, A., et al. (2016). Coseismic deformation, filed observations and seismic fault of the 17 November 2015 M_w6.5, Lefkada Island, Greece earthquake. *Tectonophysics, 687,* 210–222.

Gomberg, J., Bodin, P., & Reasenberg, P. A. (2003). Observing earthquakes triggered in the near field by dynamic deformations. *Bulletin of the Seismological Society of America, 93,* 118–138.

Got, J.-L., Fréchet, J., & Klein, F. W. (1994). Deep fault plane geometry inferred from multiplet relative relocation beneath the south flank of Kilauea. *Journal of Geophysical Research, 99,* 15375–15386. doi:10.1029/94JB00577.

Harris, R. A. (1998). Introduction to special section: stress triggers, stress shadows, and implications for seismic hazard. *Journal of Geophysical Research, 103,* 24347–24358.

Haslinger, F., Kissling, E., Ansorge, J., Hatzfeld, D., Papadimitriou, E., Karakostas, V., et al. (1999). 3D crustal structure from local earthquake tomography around the gulf of Arta (Ionian region, NW Greece). *Tectonophysics, 304,* 201–218.

Hatzfeld, D., Kassaras, I., Panagiotopoulos, D., Amorese, D., Makropoulos, K., Karakaisis, G., et al. (1995). Microseismicity and strain pattern in northwestern Greece. *Tectonics, 14,* 773–785.

Ilieva, M., Briole, P., Ganas, A., Dimitrov, D., Elias, P., Mouratidis, A., et al. (2016). Fault plane modeling of the 2003 August 14 Lefkada Island (Greece) earthquake based on the analysis of ENVISAT SAR interferograms. *Tectonophysics, 693,* 47–65. doi:10.1016/j.tecto.2016.10.021.

Kagan, Y. Y. (1991). 3-D rotation of double-couple earthquake sources. *Geophysical Journal International, 106,* 709–716. doi:10.1111/j.1365-246X.1991.tb06343.x.

Karakostas, V. G., & Papadimitriou, E. E. (2010). Fault complexity associated with the 14 August 2003 M_w6.2 Lefkada, Greece, aftershock sequence. *Acta Geophysica, 58,* 838–854. doi:10.2478/s11600-010-0009-6.

Karakostas, V. G., Papadimitriou, E. E., & Gospodinov, D. (2014). Modeling the 2013 North Aegean (Greece) seismic sequence: geometrical and frictional constraints, and aftershock probabilities. *Geophysical Journal International, 197,* 525–541. doi:10.1093/gji/ggt523.

Karakostas, V. G., Papadimitriou, E. E., Karakaisis, G. F., Papazachos, C. B., Scordilis, E. M., Vargemezis, G., et al. (2003). The 2001 Skyros, northern Aegean, Greece, earthquake sequence: off-fault aftershocks, tectonic implications, and seismicity triggering. *Geophysical Research Letters, 30*(1), 1012. doi:10.1029/2002GL015814.

Karakostas, V., Papadimitriou, E., Mesimeri, M., Gkarlaouni, Ch., & Paradisopoulou, P. (2015). The 2014 Kefalonia doublet (Mw6.1 and Mw6.0) central Ionian Islands, Greece: seismotectonic implications along the Kefalonia transform fault zone. *Acta Geophysica, 63,* 1–16. doi:10.2478/s11600-014-0227-4.

Karakostas, V. G., Papadimitriou, E. E., & Papazachos, C. B. (2004). Properties of the 2003 Lefkada, Ionian Islands, Greece, earthquake seismic sequence and seismicity triggering. *Bulletin of the Seismological Society of America, 94,* 1976–1981.

Kikuchi, M., & Kanamori, H. (1991). Inversion of complex body waves–III. *Bulletin of the Seismological Society of America, 81,* 2335–2350.

Kiratzi, A. A., & Langston, C. (1991). Moment tensor inversion of the January 17, 1983 Kefallinia event of Ionian Islands. *Geophysical Journal International, 105,* 529–535.

Kissling, E., Ellworth, W. L., Eberhart-Phillips, D., & Kradolfer, U. (1994). Initial reference models in local earthquake tomography. *Journal of Geophysical Research, 99,* 19635–19646.

Klein, F. W. (2000). User's Guide to HYPOINVERSE-2000, a Fortran program to solve earthquake locations and magnitudes. *US Geological Survey*. doi:10.13140/2.1.4859.3602. **(Open File Report 02–171 Version 1.0.)**.

Kokinou, E., Papadimitriou, E., Karakostas, V., Kamberis, E., & Vallianatos, F. (2006). The Kefalonia transform zone (offshore western Greece) with special emphasis to its prolongation towards the Ionian abyssal plain. *Marine Geophysical Researches, 27,* 241–252.

Louvari, E., Kiratzi, A. A., & Papazachos, B. C. (1999). The Cephalonia transform fault and its extension to western Lefkada island (Greece). *Tectonophysics, 308,* 223–236.

Melgar, D., Ganas, A., Geng, J., Liang, C., Fielding, E. J., & Kassaras, I. (2017). Source characteristics of the 2015 M_w6.5 Lefkada, Greece, strike–slip earthquake. *Journal of Geophysical Research*. doi:10.1002/2016JB013452.

Papadimitriou, E. E. (1993). Focal mechanism along the convex side of the Hellenic Arc and its tectonic significance. *Bollettino Di Geofisica Teorica Ed Applicata, 35,* 401–426.

Papadimitriou, E. E. (2002). Mode of strong earthquake occurrence in central Ionian Islands (Greece). Possible triggering due to Coulomb stress changes generated by the occurrence of previous strong shocks. *Bulletin of the Seismological Society of America, 92,* 3293–3308.

Papazachos, B. C., Karakaisis, G. F., and Hatzidimitriou, P. M. (1994). Further information on the transform fault of the Ionian Sea. XXIV General Assembly of the European Seismology Commission, Athens, 19–24 September, p. 12.

Papazachos, B. C., Kiratzi, A. A., & Karakostas, B. G. (1997). Towards a homogeneous moment magnitude determination for earthquakes in Greece and the surrounding area. *Bulletin of the Seismological Society of America, 87,* 474–483.

Papazachos, B. C., & Papazachou, C. C. (2003). *The earthquakes of Greece* (p. 304). Thessaloniki: Ziti Publication Co.

Permanent Regional Seismological Network (1981) operated by the Aristotle University of Thessaloniki, doi:10.7914/SN/HT.

Rice, J., & Cleary, M. (1976). Some basic stress diffusion solutions for fluid saturated elastic porous media with compressible constituents. *Reviews of Geophysics, 14,* 227–241.

Schaff, D. P., Bokelmann, G. H. R., Ellsworth, W. L., Zanzerkia, E., Waldhauser, F., & Beroza, G. C. (2004). Optimizing correlation techniques for improved earthquake location. *Bulletin of the Seismological Society of America, 94,* 705–721.

Schaff, D. P., & Waldhauser, F. (2005). Waveform cross-correlation-based differential travel-time measurements at the northern California seismic network. *Bulletin of the Seismological Society of America, 95,* 2446–2461.

Scholz, C. H. (2002). *The mechanics of earthquakes and faulting* (p. 503). Cambridge: Cambridge University Press.

Scordilis, E. M., Karakaisis, G. F., Karakostas, B. G., Panagiotopoulos, D. G., Comninakis, P. E., & Papazachos, B. C. (1985). Evidence for transform faulting in the Ionian Sea: the Cephalonia Island earthquake sequence. *Pure and Applied Geophysics, 123,* 388–397.

Sokos, E. N., & Zahradnik, J. (2008). ISOLA a Fortran code and a Matlab GUI to perform multiple-point source inversion of seismic data. *Computers & Geosciences, 34,* 967–977. doi:10.1016/j.cageo.2007.07.005.

Sokos, E. N., & Zahradnik, J. (2013). Evaluating centroid-moment-tensor uncertainty in the new version of ISOLA software. *Seismological Research Letters, 84,* 656–665. doi:10.1785/0220130002.

Sokos, E., Zahradnik, J., Gallovic, F., Serpetzidaki, A., Plicka, V., & Kiratzi, A. (2016). Asperity break after 12 years: the M_w6.4 2015 Lefkada (Greece) earthquake. *Geophysical Research Letters, 43,* 6137–6145. doi:10.1002/2016GL069427.

Stamatelos, J. N. (1870). The thirteen mentioned destructions of Lefkada, from 1612 till 1869. Ephimeris of Philomathon, Athens 24 January 1870, 726, (in Greek).

Waldhauser, F. (2001). HypoDD—a program to compute double-difference hypocenter locations, US Geological Survey Open File Report, pp. 01–113.

Waldhauser, F., & Ellsworth, W. L. (2000). A double-difference earthquake location algorithm: method and application to the Northern Hayward Fault California. *Bulletin of the Seismological Society of America, 90,* 1353–1368.

Wessel, P., & Smith, W. H. F. (1998). New, improved version of the generic mapping tools released. *EOS, Transactions American Geophysical Union, 79,* 579.

(Received April 14, 2017, revised June 15, 2017, accepted June 23, 2017)